An Analytical Framework for Quadrilateral Surface Mesh Improvement with an Underlying Triangulated Surface Definition

Kiran Shivanna[1], Nicole Grosland[2], and Vincent Magnotta[3]

[1] Center for Computer Aided Design, The University of Iowa
kiran-shivanna@uiowa.edu
[2] Department of Biomedical Engineering, The University of Iowa
nicole-grosland@uiowa.edu
[3] Department of Radiology, The University of Iowa
vincent-magnotta@uiowa.edu

Summary. Surface mesh quality plays a very important role in the solution accuracy and in the quality of the ensuing volumetric mesh. Amongst the techniques available, optimization based methods are commonly used for mesh quality improvement. Optimization methods for volumetric and planar surface mesh quality improvement are very well researched. However, this is not true for non-planar meshes. In this manuscript, we focus on quadrilateral non-planar surface meshes obtained during hexahedral mesh generation of anatomic structures. A modified untangling function based on node normals for quadrilateral elements is proposed. A parameterization-based method available is enhanced by giving it an analytical framework. A new projection-based method is proposed and its performance is comparable to the parametric method. The results of the enhanced/proposed methods are superior to the results obtained from Laplacian smoothing.

Key words: finite element method, mesh improvement, optimization, anatomic structures

1 Introduction

Finite element analysis (FEA) is the most commonly used method in numerical simulations due to its wide range of applicability and versatility in representing complex structures. One of the most influential factors governing solution accuracy is mesh quality. Proper care should be taken during mesh generation to ensure that a mesh of high quality is created. As the geometry of the structure becomes more complex, there is an increased probability

that elements of poor quality may exist, as is frequently encountered with anatomic structures. Several mesh generation and mesh improvement algorithms for volumetric meshing rely on the surface node definitions to compute the interior node locations. Consequently, in order to achieve a solid mesh of high quality, it is imperative that the quality of the surface mesh be superior. Moreover, these surface nodes are often constrained during volumetric mesh generation and mesh improvement. For example, mesh generation algorithms such as the advancing front method [1] initiate with surface elements to fill the volume. For multiblock meshing methods [2], the surface nodes at the individual block level are constrained while the interior nodes are interpolated. As a result, the quality of the interpolation is directly dependent on the location of the surface nodes. In volumetric mesh improvement methods [3, 4], the surface nodes are generally constrained while the interior nodes are moved to optimal positions. Constraining the surface nodes directly links the overall mesh quality to the surface mesh quality. In addition, boundary conditions are applied at the surface and field variables of interest are often measured at/near the surface, thus further influencing the solution quality.

Mesh improvement can be achieved using techniques based on node reconnection [5] and node repositioning/movement [3, 4]. Node reconnection based techniques improve mesh quality by introducing additional nodes, eliminating existing nodes, and altering the element connectivity as required. Simplest amongst the node movement based methods is Laplacian smoothing [6], a heuristic based method in which the node of interest is moved to the geometric center of the connected nodes. Even though Laplacian smoothing distributes the nodes uniformly, it does not guarantee a valid mesh. This led to mesh improvement using optimization techniques [3, 4].

Optimization techniques rely on a systematic approach to achieve optimum mesh quality. During optimization, an objective function is minimized. The minimization may be subject to a given set of constraints. For example, during mesh improvement, a function representing a quality measure is optimized. This optimization process establishes the direction of node movement that ultimately improves the mesh quality. Amongst the various metrics available, the unconstrained minimization of Jacobian based measures are commonly used. The mesh quality metrics and mesh improvement procedures are well established for planar surface [7] and continuum mesh definitions [8]. However, the applicability of the quality metrics and mesh improvement procedures to non-planar surface meshes are still being explored.

Various criteria have been reported in the literature to check for the validity of a quadrilateral surface mesh. Chen et al. [9] consider an element to be inverted if the dot product between the normal of the underlying surface and the mesh is less than zero. Yin et al. [10] use the centroid of the volume element (hexahedron) as a guide to determine if the surface quadrilateral is tangled. This method will not be applicable; if we have only a surface mesh or the location of interior nodes of volume meshes are not valid. Hence, a method that depends only on the node normal information would be preferrable in un-

tangling surface meshes. Towards improving the quality of the surface mesh, we have developed a modified untangling function.

Techniques available for non-planar mesh improvement start with the construction of a local space. Knupp [7] and Frey et al. [11] use the tangent plane at the node of interest as the local space for the node movement. Zhang et al. [12] use a plane that encompasses normal and tangent direction at the node of interest. Escobar et al. [13] use a local space obtained by projecting the elements sharing a given node, onto a best fit plane. Yin et al. [10] consider a quadratic surface function obtained by fitting the neighborhood nodes. Each of the aforementioned techniques moves the nodes off the surface. Garimella et al. [14] consider the parametric space of the underlying surface element as the local space, thus tracking the node movement exclusively along the surface. The work in this paper builds upon the concepts described by Garimella et al. [14]. The parametric space method can also be used to improve surface meshes with n-sided polygons [15]. In this paper, we restrict ourselves to quadrilateral surface meshes with an underlying triangulated surface definition encountered while generating all-hexahedral meshes of anatomic structures. For example, the surface nodes in multiblock meshing [2] are projected onto the underlying triangulated surface definition using closest-point projection. The optimality of the projected node distribution is dependent on the curvature of the underlying surface definition. Regions of high curvature generally have sub-optimal node distribution thus necessitating the use of surface mesh improvement techniques.

This manuscript is organized as follows. The Jacobian of a non-planar element is computed through rigid transformation (Section 2.1). The mesh improvement method used here consists of two stages: (1) untangling and (2) shape improvement. A modified untangling function that incorporates the node normal is proposed for quadrilateral mesh definitions (Section 2.2) and Jacobian matrix condition number is used for the shape improvement (Section 2.3). The analytic differentiation of the mesh quality metrics in parametric and physical space for optimization direction computation is implemented (Section 2.4 and Appendix). If the underlying surface is triangulated as is the case here, parameterization is not required. Hence, an alternate optimization strategy based on projection has been proposed (Section 2.4). An optimization path computation based on the intersection of the optimization direction with the edges of the underlying surface elements is implemented (Section 2.5). A simple 2D example (Section 2.6) and several 3D examples (Section 3) demonstrating the capability of the proposed methods are presented.

2 Methods

The methods used in mesh improvement are described in the subsequent paragraphs. To avoid any confusion in the description, the underlying triangulated surface definition is referred to as the *surface*, the points defining the surface

as *vertices*, and triangles defining the surface as *cells*. The quadrilateral surface whose quality needs to be improved will be referred to as the *mesh*, points defining the mesh as *nodes*.

2.1 Jacobian of a Triangle in 3D

The Jacobian based quality metrics are used in the quality improvement. The Jacobian of a triangle in 3D/physical space is a 3X2 matrix and that of a triangle in 2D/computational/parametric space is a 2X2 matrix. Hence, the above mentioned mesh quality metrics are easily computed for a triangle in 2D space. To calculate the quality metric of a triangle in 3D, the triangle is rigidly transformed so that all the nodes lie in a 2D plane. This transformation will not change the above mentioned mesh quality metric values, as the determinant and the condition number of the Jacobian are orientation invariant. The transformation is as follows.

A triangle in 3D is defined by its three nodes, P_1, P_2 and P_3, with edge lengths l_1, l_2 and l_3 as shown in Fig. 1. The transformed triangle in 2D is defined by nodal positions p_1, p_2 and p_3, respectively. The 2D coordinates are defined as follows: $p_1 = (0, 0)$, $p_2 = (l_1, 0)$ and $p_3 = (x, y)$. The values for x and y can be computed in terms of edge lengths as,

$$x = \frac{l_3^2 - l_2^2 + l_1^2}{2l_1} \tag{1}$$

$$y = \sqrt{l_3^2 - x^2} \tag{2}$$

The Jacobian matrix for the triangle at node p_1 is,

$$J_{P_1} = \begin{pmatrix} l_1 & x \\ 0 & y \end{pmatrix} \tag{3}$$

The Jacobian matrices at the nodes P_2 and P_3 are given in Appendix (Equation 14).

2.2 Untangling

For a quadrilateral, the Jacobian based mesh quality metrics are evaluated by decomposing the quadrilateral into four triangles.The mesh quality of the decomposed triangles are evaluated by the method described in Section 2.1. The mesh quality measure used in untangling the planar meshes [3] was modified to untangle non-planar quadrilateral meshes. Consider the quadrilateral shown in Fig.2. Let the node of interest be P_3. Four triangles 1, 2, 3 and 4 can be formed by decomposing the quadrilateral. With the movement of node P_3, the quality of triangles 2, 3 and 4 are affected while triangle 1 (referred to as the dead zone in the literature [9]) is unaffected.

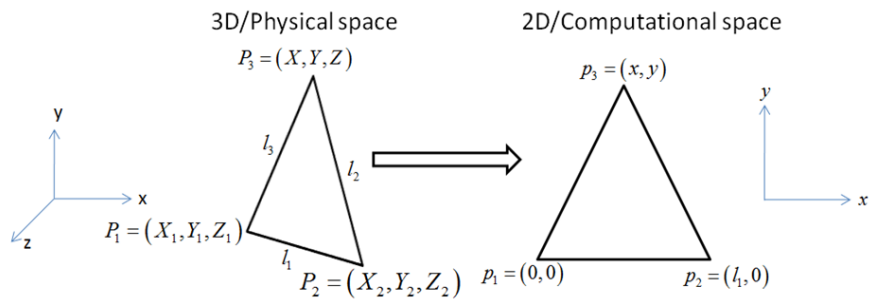

Fig. 1. Physical space to computational space transformation for Jacobian computation. The triangles are obtained by decomposing a quadrilateral into triangles.

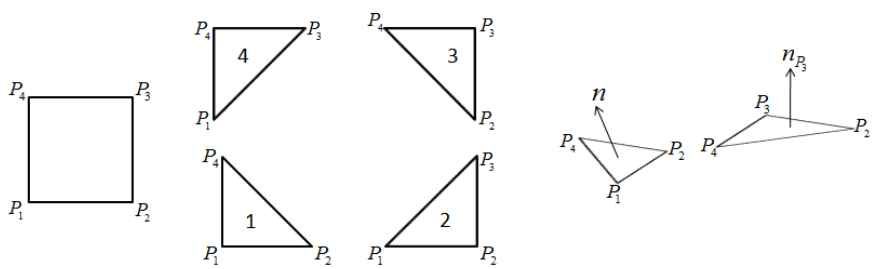

Fig. 2. Decomposition of a quadrilateral element into four triangles for the computation of mesh quality metrics.

The objective function for triangle 3 with node P_3 as the reference node (where mesh quality is measured) is,

$$f_{P_3} = abs(\alpha_{P_3}) - \alpha_{P_3} \tag{4}$$

where α_{P_3} is defined as

$$\alpha_{P_3} = (n \cdot n_{P_3} - cos(\theta))|J_{P_3}| \tag{5}$$

n is the normal of triangle 1, and n_{P_3} is the normal of triangle 3 given by

$$n_{P_3} = \overrightarrow{P_2P_3} \times \overrightarrow{P_2P_4} \tag{6}$$

θ is user defined and may vary depending on the curvature of the mesh. The range of θ is between 0^0 and 180^0. $|J_{P_3}|$ is the determinant of the Jacobian. Equations can similarly be written for triangles 2 and 4 whose reference nodes are P_2 and P_4 respectively.

From Equation 5, the decrease in the orientation difference between triangle 1 and triangle 3 increases $(n \cdot n_{P_3})$ thus increasing α_{P_3}. The dot product is a measure of the cosine of the angle between the normals of triangle 1 and triangle 3. With the decrease in the angle, the co-planarity of the nodes

increases. The normals of the triangles are oriented such that the mesh is untangled. It can be shown that for a planar mesh, the term $n \cdot n_{P_i}$ is -1 if the triangles are flipped, thus making the method applicable to both planar and non-planar meshes.The mesh is considered when the objective function evaluates to zero at all the nodes of the mesh.

2.3 Shape Improvement

When once the mesh is untangled, the mesh quality is further improved using condition number as the objective function in optimization. The equation for the condition number κ is,

$$\kappa_{P_i} = \frac{\|J_{P_i}\|^2}{2|J_{P_i}|} \tag{7}$$

where $\|J_{P_i}\|$ is the Frobenius norm at point P_i. It should be noted that the determinant of the Jacobian is node invariant, but the Frobenius norm is not. Thus, the Frobenius norm varies with the node considered and the values at the nodes of the triangle considered are given in Appendix (Equation 16). The condition number is a function of the included edge lengths of a given node and the area of the triangle considered, thereby making the condition number orientation invariant. With the objective functions computed, the optimization direction and step length need to be computed. The computations are described in Section 2.4 and Section 2.5 respectively.

2.4 Optimization Path Computation

Optimization Direction Computation

The Jacobian metrics used in the objective function/mesh quality metrics (Section 2.2 and 2.3) are the determinant of the Jacobian $|J_{P_i}|$ and the Frobenius norm $\|J_{P_i}\|$. The solution to the optimization problems often require methods that are based on the gradient (e.g., gradient descent and conjugate gradient) of an objective function. Here, optimization direction computation is done using (1) parameterization-based and (2) projection-based methods.

Parameterization-based Method

In the literature [14], the gradient is computed numerically in the parametric space. Here, an analytic gradient computation for untangling and shape improvement is used. Barycentric mapping is used for parameterization between physical and parametric coordinates. The parameterization of the local space, constrains the node movement to the underlying surface. Consider a triangular cell on which the reference node $P_i = (X, Y, Z)$ lies (Fig. 3). The corresponding location of P_i in the parametric space is $r_i = (\xi_i, \eta_i)$. The 3D physical coordinates of the cell are X, Y and Z and the 2D local parametric

space coordinates are ξ and η. The vertices of the cell in the physical coordinates are $Q_1 = (S_1, T_1, U_1)$, $Q_2 = (S_2, T_2, U_2)$ and $Q_3 = (S_3, T_3, U_3)$ and in the parametric space are $r_1 = (\xi_1, \eta_1)$, $r_2 = (\xi_2, \eta_2)$ and $r_3 = (\xi_3, \eta_3)$. The optimization direction in the parametric space for the untangling function is given by,

$$\frac{\partial}{\partial \xi}(f_{P_i}) = \frac{\partial}{\partial X}(f_{P_i})\frac{\partial X}{\partial \xi} + \frac{\partial}{\partial Y}(f_{P_i})\frac{\partial Y}{\partial \xi} + \frac{\partial}{\partial Z}(f_{P_i})\frac{\partial Z}{\partial \xi} \tag{8}$$

and for the shape improvement is given by,

$$\frac{\partial}{\partial \xi}(\kappa_{P_i}) = \frac{\partial}{\partial X}(\kappa_{P_i})\frac{\partial X}{\partial \xi} + \frac{\partial}{\partial Y}(\kappa_{P_i})\frac{\partial Y}{\partial \xi} + \frac{\partial}{\partial Z}(\kappa_{P_i})\frac{\partial Z}{\partial \xi} \tag{9}$$

Similar equations can be written with respect to η. Computation of derivatives of untangling and shape improvement functions in the physical coordinates is straightforward and the details are given in Appendix (Equations 17 to 22).

The barycentric map is computed as,

$$X = \frac{\langle r_i, r_1, r_2\rangle S_3 + \langle r_i, r_2, r_3\rangle S_1 + \langle r_i, r_3, r_1\rangle S_2}{\langle r_1, r_2, r_3\rangle} \tag{10}$$

where, $\langle , , \rangle$ represents the area of the triangle given by the three coordinates of interest. Similar equations can be written for Y and Z coordinates. The derivatives of physical coordinates w.r.t. parametric coordinates are,

$$\frac{\partial X}{\partial \xi} = \frac{1}{2}\frac{(\eta_1 - \eta_2)S_3 + (\eta_2 - \eta_3)S_1 + (\eta_3 - \eta_1)S_2}{\langle r_1, r_2, r_3\rangle} \tag{11}$$

$$\frac{\partial X}{\partial \eta} = \frac{1}{2}\frac{(\xi_1 - \xi_2)S_3 + (\xi_2 - \xi_3)S_1 + (\xi_3 - \xi_1)S_2}{\langle r_1, r_2, r_3\rangle} \tag{12}$$

Similar equations can be written for Y and Z coordinates.

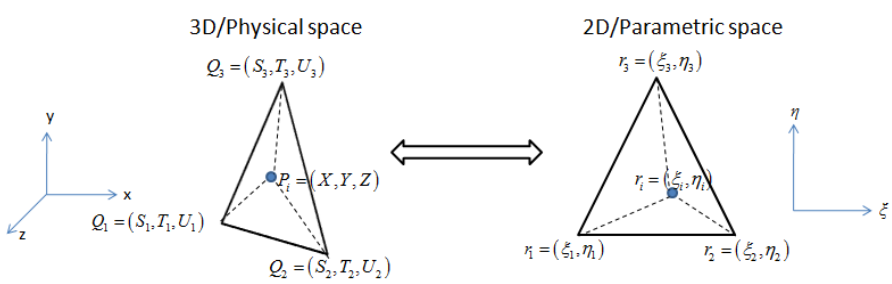

Fig. 3. Barycentric mapping of a triangular cell between physical space and parametric space. Reference node P_i lies on the triangular cell.

Projection-based Method

If the computation of the gradient of an objective function is done in physical space as is the case in the projection-based method, the gradient direction could point away from the underlying surface. To constrain the optimization direction onto the underlying triangulated surface, the original direction vector is projected orthogonally onto the plane containing the triangular cell on which the node of interest lies (Fig. 4a). The projected direction vector would establish the modified direction for the node movement. The orthogonal projection can be computed as,

$$M = D - (D \cdot N)N \tag{13}$$

where, M is the projected direction vector on the triangular cell on which the node lies, D is the original optimization direction vector in the physical space and N is the unit normal of the triangular cell on which the node lies. The optimization direction vector D is computed from the equations given in Appendix (Equations 20 to 22). From Fig. 4b, $(D{\cdot}N)$ represents the magnitude of the orthogonal projection of D on N. Equation 13 is obtained from vector subtraction (Fig. 4b).

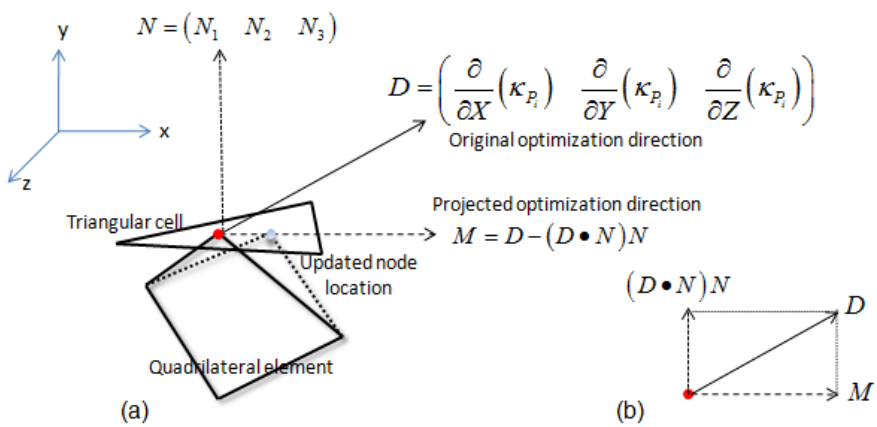

Fig. 4. Projection of optimization direction in physical space: (a) pictorial representing the projection process onto a triangular cell, (b) computation of projection direction using vector subtraction.

2.5 Step Length Computation

Step length need to be determined for the optimization direction computed in Section 2.4 and the procedure is as follows. The distance between the intersection point of the optimization direction with one of the edges of the cell and

the current node location would serve as the initial step length. The objective function is evaluated at the intersection point. If the objective function decreases, the neighboring cell is considered for the minimization direction computation. Otherwise, the step length is decreased until the optimum result is obtained.

The starting location of the node to be smoothed or the intersection point obtained during mesh improvement can lie in one of the three locations, (1) on a vertex of the surface (Fig. 5a), (2) on an edge of a cell (Fig. 5b), and (3) interior to a cell (Fig. 5c). If the step length is negligible, it implies that the current location is the optimum location for the node and the cell on which the node lies. To continue mesh improvement, for a node located (1) on a vertex of the surface, the neighboring cells sharing the vertex are checked for the subsequent path computation; (2) on an edge of a cell, the neighboring cell sharing the edge on which the node is located is used for the subsequent path computation; and (3) interior to a cell, the current location is the optimum location.

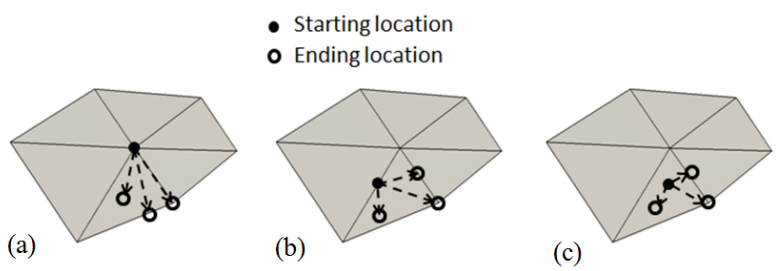

Fig. 5. Optimization path computation with possible starting and ending locations of a node. Starting location: (a) close to a vertex on the underlying mesh, (b) on an edge of the triangular cell, and (c) interior to a triangular cell.

2.6 2D Example

The parameterization-based and the projection-based methods are evaluated with a simple 2D example. The mesh and the underlying surface are shown in Fig. 6a. The mesh contains 9 nodes ($P_1 to P_9$) and 4 quadrilateral elements. The underlying surface is triangulated. In Fig. 6b node P_5 is intentionally moved to a location making quadrilateral $P_5P_4P_2P_1$ invalid. The modified untangling function proposed cannot be evaluated if any three or more nodes of a quadrilateral are collinear or any two or more nodes of a quadrilateral are coincident. The normal evaluation would not be possible, thus precluding the use of the untangling function. If collinear or coincident nodes are found prior to the mesh improvement, the nodes are perturbed slightly from their position and projected back onto the underlying surface. But if collinear nodes

are found during the untangling phase, the following procedure is followed. While untangling, the node is moved to the location of vertex V_1 (Fig. 6c (inset)). This makes the nodes P_4, P_5 and P_2 collinear and hence untangling function cannot be computed for the subsequent iterations. To overcome the drawback, the node is perturbed in the positive and the negative directions of the coordinates of the neighboring cells (as determined in section 2.5). The perturbation is along the physical coordinates for the projection-based and along the parametric coordinates for the parameterization-based direction computation. The perturbed location that reduces the objective function is chosen for the subsequent iterations (Fig. 6c). The path traversed by the node during shape improvement is shown in Fig. 6d. The complete path taken by the node during optimization is shown in Fig. 6e (inset).

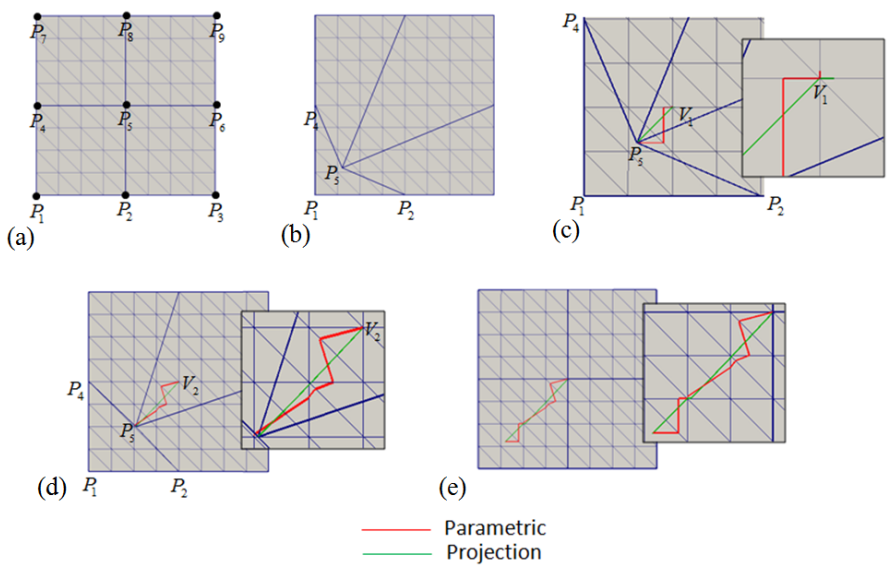

Fig. 6. Test example to evaluate parametric and projection-based optimization direction computation with a simple 2D example: (a) valid mesh with nine nodes and four quadrilaterals, (b) initial invalid mesh, (c) untangling path computation, (d) shape improvement path computation, and (e) combined optimization path.

2.7 Evaluation of Mesh Improvement Techniques

For the mesh improvement, local optimization with gradient descent was chosen as the optimization method. Three examples, (1) phalanx bone (Fig. 7), (2) femur (Fig. 8) and (3) posterior portion of sheep vertebrae (Fig. 9) were considered for mesh improvement. The example meshes were smoothed using parameterization-based method, projection-based method and Laplacian

smoothing. A value of 90^0 was assumed for θ (Equation 5) during untangling. The meshes were improved until the solution converged. The solution was deemed to have converged, when the largest displacement of all the nodes repositioned was less than $(\frac{1}{100})^{th}$ of the starting average edge length. The starting average edge length values are given in Table 1. The underlying surfaces for the three examples are shown in Fig. 7a, Fig. 8a and Fig. 9a. The initial meshes (unsmooth) shown in Fig. 7b, Fig. 8b and Fig. 9b were obtained by projecting a rectilinear grid onto the underlying surface using closest point projection [2]. The Verdict library [16] was used in the computation of the mesh quality metrics.

Table 1. Mesh and surface details

Details	Phalanx bone	Femur	Sheep vertebra
Num cells (Underlying surface)	48894	226024	121605
Num elements (Mesh)	1686	5986	7564
Ave edge length	0.918	2.908	1.214

3 Results and Discussion

3.1 Results

The meshes obtained from the Laplacian smoothing are shown in Fig. 7c, Fig. 8c and Fig. 9c. The smoothed meshes using the parameterization-based method are shown in Fig. 7d, Fig. 8d and Fig. 9d. The smoothed meshes using the projection-based method are shown in Fig. 7e, Fig. 8e and Fig. 9e.

In the tables given, *Unsmoothed*, *Laplacian*, *Parametric* and *Projection* meshes are abbreviated as **U**, **L**, **Pa** and **Pr** respectively. Mesh quality histogram based on minimum scaled Jacobian and maximum condition number for the unsmoothed and smoothed meshes of phalanx bone, femur and posterior portion of sheep vertebrae are given in Table 2, Table 3 and Table 4 respectively. The minimum scaled Jacobian for a quadrilateral is the minimum of all the values and maximum condition number is the maximum of all the values measured at the four nodes of the given quadrilateral. Mesh quality statistics such as maximum, minimum, mean and standard deviation of the scaled Jacobian and the condition number for unsmooth and smooth meshes of phalanx bone, femur and posterior portion of sheep vertebra are given in Table 5, Table 6 and Table 7 respectively.

3.2 Discussion

Inverted/invalid elements in planar and volumetric meshes are the elements having non-positive Jacobian [3]. But the definition of inverted elements in a

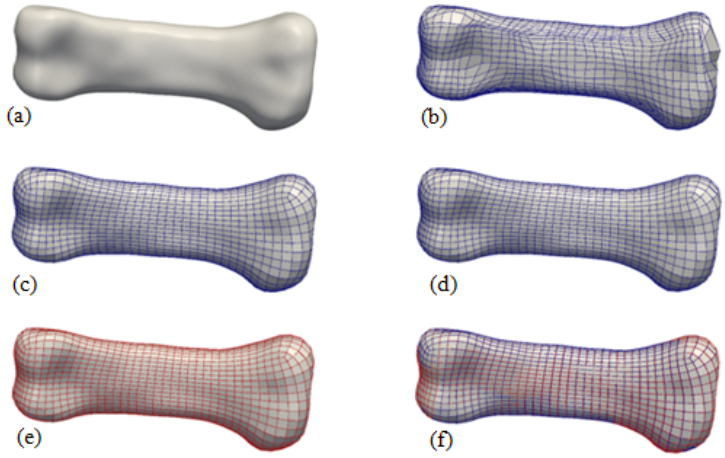

Fig. 7. Phalanx bone: (a) underlying triangulated surface definition, (b) initial unsmooth mesh, (c) smoothed mesh using Laplacian smoothing, (d) smoothed mesh using parametric method, (e) smoothed mesh using projection method, and (f) overlaid meshes from parametric and projection methods.

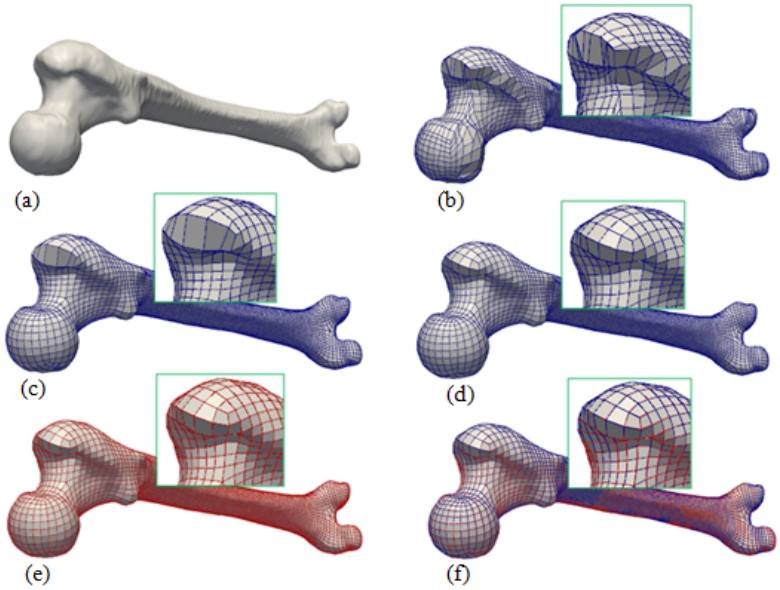

Fig. 8. Femur: (a) underlying triangulated surface definition, (b) initial unsmooth mesh, (c) smoothed mesh using Laplacian smoothing, (d) smoothed mesh using parametric method, (e) smoothed mesh using projection method, and (f) overlaid meshes from parametric and projection methods.

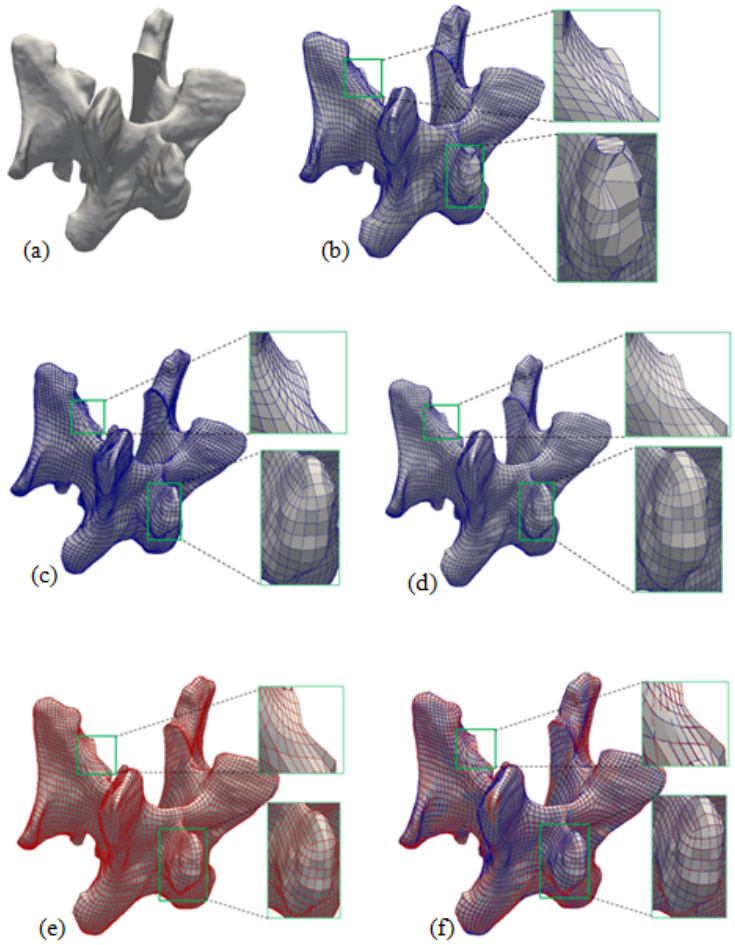

Fig. 9. Posterior portion of sheep vertebra: (a) underlying triangulated surface definition, (b) initial unsmooth mesh, (c) smoothed mesh using Lapacian smoothing, (d) smoothed mesh using parametric method, (e) smoothed mesh using projection method, and (f) overlaid meshes from parametric and projection methods. The mesh improvement is highlighted through insets.

Table 2. Mesh quality histogram for phalanx bone

Min scaled $\lvert J \rvert$	**U**	**L**	**Pa**	**Pr**	**Max κ**	**U**	**L**	**Pa**	**Pr**
$<= 0.0$	2	0	0	0	$\geq$1.0 and $<$=1.5	1300	1686	1686	1686
> 0.0 and $<= 0.1$	0	0	0	0	$>$1.5 and $<$=1.0	183	0	0	0
> 0.1 and $<= 0.2$	7	0	0	0	$>$2.0 and $<$=3.0	130	0	0	0
> 0.2 and $<= 0.4$	26	0	0	0	$>$3.0 and $<$=5.0	52	0	0	0
> 0.4 and $<= 0.6$	54	0	0	0	$>$5.0 and $<$=7.5	14	0	0	0
> 0.6 and $<= 0.8$	118	0	0	0	$>$7.5 and $<$=10.0	1	0	0	0
> 0.8 and $<= 1.0$	1479	1686	1686	1686	$>$10.0	6	0	0	0

Table 3. Mesh quality histogram for femur

Min scaled $\|J\|$	**U**	**L**	**Pa**	**Pr**	**Max κ**	**U**	**L**	**Pa**	**Pr**
<= 0.0	22	0	0	0	≥1.0 and <=1.5	3841	5960	5970	5980
> 0.0 and <= 0.1	11	0	0	0	>1.5 and <=1.0	1733	24	16	6
> 0.1 and <= 0.2	13	0	0	0	>2.0 and <=3.0	295	2	0	0
> 0.2 and <= 0.4	50	0	0	0	>3.0 and <=5.0	56	0	0	0
> 0.4 and <= 0.6	104	1	2	0	>5.0 and <=7.5	14	0	0	0
> 0.6 and <= 0.8	307	12	8	10	>7.5 and <=10.0	4	0	0	0
> 0.8 and <= 1.0	5479	5973	5976	5976	>10.0	43	0	0	0

Table 4. Mesh quality histogram for sheep vertebra(posterior)

Min scaled $\|J\|$	**U**	**L**	**Pa**	**Pr**	**Max κ**	**U**	**L**	**Pa**	**Pr**
<= 0.0	31	3	0	0	≥1.0 and ≤1.5	4610	6565	6445	6512
> 0.0 and ≤ 0.1	19	3	0	0	>1.5 and ≤1.0	1184	648	856	785
> 0.1 and ≤ 0.2	39	5	2	4	>2.0 and ≤3.0	927	236	205	201
> 0.2 and ≤ 0.4	136	45	23	22	>3.0 and ≤5.0	556	72	50	60
> 0.4 and ≤ 0.6	267	118	105	104	>5.0 and ≤7.5	136	23	7	3
> 0.6 and ≤ 0.8	911	314	339	311	>7.5 and ≤10.0	48	11	1	3
> 0.8 and ≤ 1.0	6161	7076	7095	7123	>10.0	103	9	0	0

Table 5. Mesh quality statistics for phalanx bone

	Scaled $\|J\|$				κ			
Mesh	**Min**	**Max**	**Mean**	**Std dev**	**Min**	**Max**	**Mean**	**Std dev**
U	-0.123	1.000	0.904	0.143	1.000	∞	∞	∞
L	0.849	1.000	0.993	0.016	1.000	1.296	1.075	0.080
Pa	0.848	1.000	0.993	0.016	1.000	1.255	1.071	0.066
Pr	0.847	1.000	0.993	0.016	1.000	1.242	1.071	0.063

Table 6. Mesh quality statistics for femur

	Scaled $\|J\|$				κ			
Mesh	**Min**	**Max**	**Mean**	**Std dev**	**Min**	**Max**	**Mean**	**Std dev**
U	-0.808	1.000	0.921	0.137	1.003	∞	∞	∞
L	0.516	1.000	0.988	0.022	1.000	2.256	1.211	0.138
Pa	0.582	1.000	0.986	0.023	1.000	1.787	1.212	0.135
Pr	0.622	1.000	0.985	0.022	1.000	1.642	1.211	0.132

Table 7. Mesh quality statistics for vertebra (posterior)

	Scaled $\|J\|$				κ			
Mesh	**Min**	**Max**	**Mean**	**Std dev**	**Min**	**Max**	**Mean**	**Std dev**
U	-0.849	1.000	0.882	0.172	1.000	∞	∞	∞
L	-0.634	1.000	0.952	0.104	1.000	∞	∞	∞
Pa	0.149	1.000	0.952	0.091	1.000	7.854	1.266	0.382
Pr	0.138	1.000	0.954	0.092	1.000	8.819	1.258	0.405

non-planar mesh is not clearly defined in the literature because of the difficulty associated with quantifying what constitutes an inverted element [18]. This is especially true for triangular elements. For quadrilateral elements, various criteria have been used to define an invalid element (as discussed in the Section 1) including the warping factor [17]. These criteria measure the difference in the normal orientation at the nodes of a quadrilateral element. Hence, an untangling function (Equation 5) that minimizes the difference in node normal orientations has been proposed.

During the shape improvement, different criteria are used for defining feasible/valid region for a given node. Escobar et al. [13] use the parametric space defined by the projection of sub mesh (elements sharing a given node) onto the best fit plane as the valid region. Garimella et al.[14] use an imaginary plane containing the opposing edge of the node of interest and perpendicular to the normal at the node. If the node crosses the imaginary plane during node movement, the element is considered invalid. In the proposed method, the element is considered invalid if the node movement makes the angles as computed in Equation 6 greater than the user defined value (θ in Equation 5).

A simple two dimensional problem (Fig. 6) is solved to compare the two techniques. It is seen from Fig. 6e that the two techniques converge to the same solution, but the optimization path computed is different. The projection-based optimization direction has a much straighter path to the optimal location (Vertex V_2 in Fig. 6e) than the parametric method. Three examples with varying degree of curvature change on the underlying surfaces are chosen to test the mesh improvement techniques. Curvature change is a good indicator of the uniformity of the node distribution on the unsmooth mesh and with it the initial mesh quality. In all the three cases, the unsmooth meshes contain elements with negative scaled Jacobian thus implying low mesh quality. Laplacian smoothing improves the overall quality of the meshes shown (Fig. 7c, Fig. 8c and Fig. 9c) as compared to the unsmooth meshes but does not guarantee a valid mesh in all examples. However, the parameterization-based (Fig. 7d, Fig. 8d and Fig. 9d) and projection-based (Fig. 7e, Fig. 8e and Fig. 9e) methods perform better resulting in improved mesh quality (Table 5, 6 and 7) as compared to Laplacian smoothing. For example, negative Jacobians that exist for the posterior portion of sheep vertebrae mesh obtained by Laplacian smoothing are eliminated with the techniques proposed in the paper. The results obtained between projection and parameterization-based smoothing are comparable with both the methods resulting in valid meshes.

Laplacian smoothing works well for regions on the surface with low rate of change of curvature as is the case with phalanx bone (Fig. 7). Hence, mesh quality statistics obtained through Laplacian smoothing compare favorably with projection-based and parameterization-based methods (Table 2 and Table 5). For the regions with high curvature (Fig. 8b inset), Laplacian smoothing loses the geometric fidelity (Fig. 8c inset) as compared to parametric (Fig. 8d inset) and projection (Fig. 8e inset) based methods. One more

drawback of Laplacian smoothing is that it tends to fold the mesh (Fig. 9c top-inset) in the regions of concave boundaries (Fig. 9b top-inset). The parametric (Fig. 9d top-inset) and projection-based methods (Fig. 9e top-inset) avoid mesh folding thus improving the mesh quality. Hence, mesh quality statistics for optimization methods show dramatic improvement compared with Laplacian smoothing for sheep vertebra (Table 4). Even though parametric and projection-based methods yield valid meshes, the location of nodes in a converged solution is not identical because, the optimization paths for the two methods are not identical (Fig. 6e). The contour of the objective function of an individual node is convex but the local objective function is not [19]. The local objective function can contain multiple local minima and hence the difference in the location of nodes. Fig. 7f, Fig. 8f and Fig. 9f show the overlaid meshes from parametric and projection methods for all the three examples.

If the underlying surface definition contains non-triangular elements, the elements can be triangulated and the proposed method applied. If the triangulation is not allowed, the procedure described in the literature can be used [14]. For planar and volumetric meshes, the optimization path is a straight line and can easily be stored as a vector. For non-planar meshes, the optimization path is made of segments of lines that lie on the underlying surface. The implementation of global optimization becomes difficult for non-planar meshes because, the optimization paths for all the nodes have to be stored and the intermediate locations of the nodes for fractional step lengths have to be computed. Here local optimization is used because; every node is moved to its best possible location one by one. If the node moves out of a cell, the optimization starts afresh thus simplifying the implementation.

4 Conclusion

Enhancements/new techniques for non-planar quadrilateral surface mesh improvement are presented. A modified untangling function for quadrilateral meshes based on node normals is proposed. Two techniques, (1) parameterization-based and (2) projection-based method for optimization direction computation are presented. The parameterization-based method that improves the surface mesh quality while maintaining the mesh fidelity has been enhanced and presented herein. An analytical framework for, (1) mesh quality metrics and (2) optimization direction computation in physical and parametric space has been presented. A new projection-based optimization direction computation has been devised and implemented and its performance is comparable to that of the parametric method. The proposed methods have been successfully tested on quadrilateral surface meshes with underlying triangulated surfaces. The results are superior to those obtained by the Laplacian smoothing method.

References

1. Blacker, T.D., Meyers, R.J., Seams and wedges in plastering: A 3D hexahedral mesh generation algorithm. Engineering with Computers, 1993. 2(9): p. 83-93.
2. Grosland, N.M., Shivanna, K.H., Magnotta, V.A., Kallemeyn, N.A., DeVries, N.A., Tadepalli, S.C., Lisle, C., IA-FEMesh: An open-source, interactive, multiblock approach to anatomic finite element model development. Computer Methods and Programs in Biomedicine, 2009. 94(1): p. 96-107.
3. Knupp, P., Hexahedral and tetrahedral mesh untangling. Engineering With Computers, 2001. 17(3): p. 261-268.
4. Knupp, P.M., A method for hexahedral mesh shape optimization. International Journal for Numerical Methods in Engineering, 2003. 58(2): p. 319-332.
5. Freitag, L.A., Ollivier-Gooch, C., Tetrahedral mesh improvementd using swapping and smoothing. International Journal for Numerical Methods in Engineering, 1997. 40(21): p. 3979-4002.
6. Field, D., Laplacian smoothing and delaunay triangulations. Communications in Applied Numerical Methods, 1988. 4: p. 709-712.
7. Knupp, P.M., Achieving finite element mesh quality via optimization of the Jacobian matrix norm and associated quantities. Part I- a framework for surface mesh optimization. International Journal for Numerical Methods in Engineering, 2000. 48: p. 401-420.
8. Knupp, P.M., Achieving finite element mesh quality via optimization of the Jacobian matrix norm and associated quantities. Part II- a framework for volume mesh optimization and the condition number of the Jacobian matrix. International Journal for Numerical Methods in Engineering, 2000. 48: p. 1165-1185.
9. Chen, Z., Tristano, J.R., Kwok, W., Construction of an objective function for optimization based smoothing. Engineering with Computers, 2004. 20: p. 184-192.
10. Yin, J., Teodosiu, C., Constrained mesh optimization on the boundary. Engineering with Computers, 2008. 24: p. 231-240.
11. Frey, P.J., Borouchaki, H., Geometric surface mesh optimization. Computing and Visualization in Science, 1998. 1(3): p. 113-121.
12. Zhang, Y., Bajaj, C., Xu, G., Surface smoothing and quality improvement of quadrilateral/hexahedral meshes with geometric flow. Communications in Numerical Methods in Engineering, 2007. 25(1): p. 1-18.
13. Escobar, J.M., Montero, G., Montenegro, R., Rodriguez, E., An algebraic method for smoothing surface triangulations on a local parametric space. International Journal for Numerical Methods in Engineering, 2006. 66: p. 740-760.
14. Garimella, R., Shashkov, M., Knupp, P., Triangular and quadrilateral surface mesh quality optimization using local parametrization. Computer Methods in Applied Mechanics and Engineering, 2004. 193: p. 913-928.
15. Garimella, R.V., Shashkov, M.J., Polygonal surface mesh optimization. Engineering with Computers, 2004. 20: p. 265-272.
16. Pbay P., Thompson D., Shepherd J., Knupp P., Lisle C., Magnotta V., Grosland N. New Applications of the Verdict Library for Standardized Mesh Verification Pre, Post, and End-to-End Processing. Proceedings of the 16th International Meshing Roundtable, 2007.
17. ANSYS Inc. Theory reference, Release 9.0, Chapter 13. 2004.
18. Knupp, P.M., Algebraic mesh quality metrics for unstructured initial meshes. Finite Elements in Analysis and Design, 2003. 39(3): p. 217-241.

19. Diachin, L.F., Knupp, P.M., Munson, T., Shontz, S., A comparison of two optimization methods for mesh quality improvement. Engineering with Computers, 2006. 22(2): p. 61-74.

Appendix

1. Jacobian computation

$$J_{P_2} = \begin{pmatrix} (x - l_1) & -l_1 \\ y & 0 \end{pmatrix}, \qquad J_{P_3} = \begin{pmatrix} -x & (l_1 - x) \\ -y & -y \end{pmatrix} \tag{14}$$

2. Determinant of Jacobian and Frobenius norm

$$|J_{P_1}| = |J_{P_2}| = |J_{P_3}| = |J| = l_1 y \tag{15}$$

$$\|J_{P_1}\|^2 = {l_1}^2 + {l_3}^2, \qquad \|J_{P_2}\|^2 = {l_1}^2 + {l_2}^2, \qquad \|J_{P_3}\|^2 = {l_2}^2 + {l_3}^2 \tag{16}$$

3. Untangling function derivatives

$$\frac{\partial f_{P_i}}{\partial X} = \frac{\partial \alpha_{P_i}}{\partial X}\left(\frac{abs(\alpha_{P_i})}{\alpha_{P_i}} + 1\right) \tag{17}$$

$$\frac{\partial \alpha_{P_i}}{\partial X} = n \cdot \frac{\partial n_{P_i}}{\partial X}|J_{P_i}| + (n \cdot n_{P_i} - cos(\theta))\frac{\partial |J_{P_i}|}{\partial X} \tag{18}$$

$$\frac{\partial n_{P_i}}{\partial X} = \begin{pmatrix} 0 \\ Z_2 - Z_1 \\ Y_1 - Y_2 \end{pmatrix}, \quad \frac{\partial n_{P_i}}{\partial Y} = \begin{pmatrix} Z_1 - Z_2 \\ 0 \\ Y_1 - Y_2 \end{pmatrix}, \quad \frac{\partial n_{P_i}}{\partial Z} = \begin{pmatrix} Y_2 - Y_1 \\ X_1 - X_2 \\ 0 \end{pmatrix} \tag{19}$$

4. Shape improvement function derivatives

$$\frac{\partial \kappa_{P_i}}{\partial X} = \frac{|J_{P_i}|\frac{\partial \|J_{P_i}\|^2}{X} + \frac{\partial |J_{P_i}|}{X}\|J_{P_i}\|^2}{2|J_{P_i}|^2} \tag{20}$$

$$\frac{\partial |J_{P_i}|}{\partial X} = \frac{l_1(X - X_1) - x(X_2 - X_1)}{y} \tag{21}$$

$$\frac{\partial \|J_{P_1}\|^2}{\partial X} = 2(X - X_1), \quad \frac{\partial \|J_{P_2}\|^2}{\partial X} = 2(X - X_2), \quad \frac{\partial \|J_{P_3}\|^2}{\partial X} = 2(2X - (X_1 + X_2)) \tag{22}$$

Similar equations can be written for coordinates Y and Z.